Mars 2020 Entry, Descent, and Landing System Overview

Adam Nelessen, Chloe Sackier, Ian Clark, Paul Brugarolas, Gregorio Villar, Allen Chen, Aaron Stehura, Richard Otero, Erisa Stilley, David Way*, Karl Edquist*, Swati Mohan, Cj Giovingo, Mallory Lefland

Jet Propulsion Laboratory, California Institute of Technology
4800 Oak Grove Drive
Pasadena, CA 91109
818-354-2499
Adam.P.Nelessen@jpl.nasa.gov

*NASA Langley Research Center, Hampton, VA

Abstract— Building upon the success of the Mars Science Laboratory (MSL) landing and surface mission, the Mars 2020 project is a flagship-class science mission intended to address key questions about the potential for life on Mars and collect samples for possible Earth return by a future mission. [1] Mars 2020 will also demonstrate technologies needed to enable future human expeditions to Mars. Utilizing the groundbreaking entry, descent, and landing (EDL) architecture pioneered by the MSL, [2] [3] Mars 2020 will launch in July 2020 and land on Mars in February 2021.

Like its predecessor, Mars 2020 will deliver its rover payload to the Martian surface through the use of Apollo-derived entry guidance, a 21.45 meter supersonic Disk-Gap-Band parachute, a Descent Stage powered by throttleable Mars lander engines, and the signature Sky Crane maneuver. While Mars 2020 inherits most of its EDL architecture, software, and hardware from the MSL, a number of changes have been made to correct deficiencies, improve performance, and increase the robustness of the system. For example, Mars 2020 will take advantage of the favorable atmospheric conditions of the 2020 launch opportunity to deliver a larger and more capable rover than has landed on Mars to date.

A primary focus in developing the Mars 2020 EDL system has been mitigating residual risks identified after the landing of the MSL. The Advanced Supersonic Parachute Inflation Research Experiment (ASPIRE) was performed to address new concerns about the stresses experienced by parachute canopies during inflation. Other risk reduction activities include investigating possible interactions between the parachute deployment system and the inertial measurement unit (IMU) which could lead to IMU saturation, researching the effects of airborne dust on radar ground measurements, and site-specific gravity modeling for improved fuel usage.

Several enhancements were added for Mars 2020 to improve performance. The addition of Terrain Relative Navigation (TRN) allows the system to land at sites with more hazardous terrain, enabling scientists to select from locations which have previously been considered inaccessible. Mars 2020 will utilize a Range Trigger for initiating parachute deployment, which reduces landing ellipse sizes by 40% compared to the Velocity Trigger approach used on the MSL. New EDL Camera hardware will capture high resolution and high frame rate images and videos of key events, such as parachute deployment and rover touchdown. Finally, the Mars Entry, Descent, and Landing Instrumentation 2 (MEDLI2) sensor suite will build upon the successful MSL MEDLI experiment with the addition of heatshield pressure sensors tuned for the supersonic flight regime and backshell instrumentation.

The team has faced new and unexpected challenges throughout development. Notably, the failure of the flight heatshield during a static load test has prompted the fabrication of a new unit. Also, in accommodating the first ever Mars Helicopter under the rover belly pan, the EDL design has been further constrained by reduced ground clearances. Despite these challenges, much of the EDL-related hardware and software have already been delivered, and the EDL verification and validation program is on track to be completed on schedule prior to launch in July 2020.

TABLE OF CONTENTS

1. MARS 2020 OVERVIEW

Mission and Science Objectives

The Mars 2020 project is a flagship-class science mission intended to address key questions about the potential for life on Mars. Furthermore, as the first leg of a possible sample return campaign, the Mars 2020 mission will also collect samples for possible Earth return by a future mission. The sample return architecture is favorable in that it would allow for samples collected by the rover to be investigated in depth in a full-fledged laboratory setting on Earth.

The scientific goals of the Mars 2020 mission are twofold: searching both for signs of past habitable Martian conditions and signatures of ancient microbial life. Furthermore, this mission will also address the scientific objective of preparing for eventual human missions to Mars. This objective is met through executing experiments and technology demonstrations such as utilizing the Martian atmosphere for the production of oxygen, searching for resources needed to support human activities (like subsurface water),

characterizing the Martian atmosphere and climate, and EDL techniques to support landing heavier loads with less disturbance (an initiative that began with the MSL landing in 2012).

As a successor to the MSL, Mars 2020 benefits from significant flight heritage and experience, resulting in risk reduction, cost savings and an opportunity to build on previous expertise and improve the overall design. The timing of the launch opportunity in July of 2020 makes use of the fact that at that point, the distance is minimized between Earth and Mars, resulting in a more inexpensive trip.

While the mission makes use of the flight heritage from the MSL, several new and notable improvements allow for the landing of a larger rover (increase in mass from 900 to 1,050 kg) intended to travel greater distances throughout the mission, and in a more scientifically interesting location. The addition of the Terrain Relative Navigation (TRN) EDL technology enables the rover to autonomously select its precise landing location, navigating around hazardous terrain. This, in turn, allows the science team greater leeway in choosing a landing site, as they can select a locale with a higher concentration of rocks of scientific interest that would have previously deemed the site too risky. Once landed, the Mars 2020 rover has an improved mobility system, featuring a robust new wheel design intended to carry the rover longer distances (5 to 20 km). Furthermore, the rover itself features new drill technology to collect core samples of rocks and soils and cache them on the Martian surface. [4] [5]

2020 Launch Opportunity

Another EDL performance enhancement (and one classified as a "no cost" improvement) comes in the form of the favorable launch and entry windows. The Martian atmosphere in February 2021 (the time of entry) provides a highly conducive environment for an entry vehicle to fly in.

The meteorological conditions will be favorable in terms of the pressure cycle. As a result of the Martian planet's obliquity and eccentricity, a seasonal CO_2 transfer occurs from the polar caps into the atmosphere. As shown in Figure 1 by the blue trendline, this phenomena creates a significantly denser atmosphere than what was observed during the MSL entry window. A denser atmosphere translates into an increased ability to land at higher elevations, opening up more potential landing sites. Further nuances to this capability include the ability to fly the same landed mass at a higher altitude while preserving more propellant. This improvement could also extend the EDL timeline by roughly 30 seconds. Additionally, the red trendline in Figure 1 shows that an entry window of February 2021 coincides with a particularly low risk of dust events, mitigating entry concerns relating to flying through dust storms.

2. EDL SYSTEM ARCHITECTURE

Vehicle Configuration

The execution of EDL involves many different components and configurations of the spacecraft. The spacecraft that formally begins EDL consists of a cruise stage, an entry aeroshell (comprised of the heatshield and the backshell), a Descent Stage (DS), and the rover (shown in Figure 2). The DS and the rover are contained within the aeroshell.

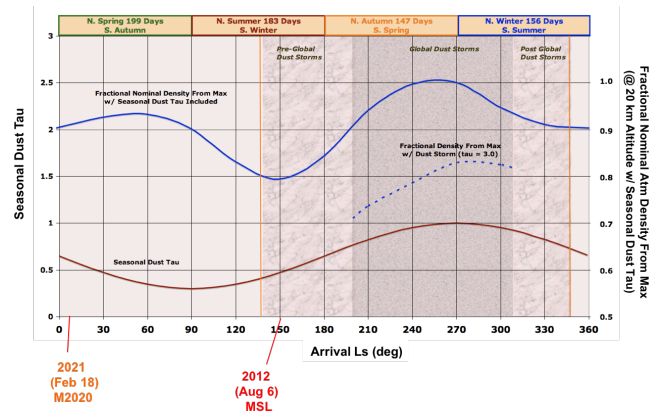The cruise stage and aeroshell are conjoined during the

Figure 1. **Mean Atmospheric Density Variability with Ls**

spacecraft's flight to Mars, but get separated just prior to entry. Two Cruise Balance Masses (CBMs) are jettisoned to offset the center of mass and create a lift vector. The entry vehicle, defined as the DS and rover inside of the aeroshell, flies a guided lifting entry until parachute deploy.

After parachute deploy, heatshield separation exposes the Powered Descent Vehicle (PDV), defined as the combination of the DS and the rover. The DS includes the terminal descent sensor (TDS), the terrain relative navigation (TRN) hardware, the Mars Lander Engines (MLEs), and the bridle umbilical device (BUD.) This assembly descends under the parachute until backshell separation, after which powered descent begins.

At a certain point during powered descent, the Sky Crane maneuver begins, wherein the rover is lowered from the DS by the BUD, simultaneously deploying its mobility system. After touchdown, the bridles are cut and the DS executes a Flyaway maneuver. The following section describes the EDL sequence of events in greater detail.
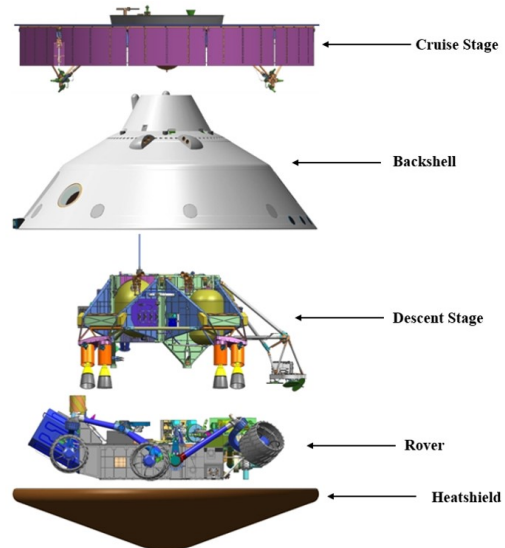

Figure 2. **Vehicle Configuration**

EDL Sequence of Events

The EDL sequence of events for Mars 2020, shown in Figure 3, follows the same heritage design as what was successfully

flown on the MSL. This section serves as a brief review of the EDL timeline, calling out the specific phases of flight and their respective triggers.

Approach—The approach phase is characterized by navigation efforts to deliver the spacecraft to the desired entry conditions. This is accomplished through a series of trajectory correction maneuvers (TCMs) that occur en route to Mars. Requirements are set on the landed position error that is derived from approach navigation (from delivery error and knowledge error). The entry vehicle possesses an amount of control authority greater than the requirement on targeting uncertainty, allowing the vehicle to fly out targeting errors during EDL.

EDL Start— EDL Start is characterized by a number of activities: the execution of a final TCM, if deemed necessary, preheating the entry propellant and engine and thruster catalyst beds, initializing the vehicle attitude knowledge, and venting the heat rejection system (HRS). The separation from the cruise stage occurs 10 minutes before the entry interface.

Exo-atmospheric—During the exo-atmospheric phase, after cruise stage separation, the vehicle enables Guidance, Navigation and Control (GNC), executes a despin from the 2 RPM cruise rate to zero rate, and turns to the entry attitude. This maneuvering is performed by Reaction Control System (RCS) thrusters. Five minutes prior to entry interface, the vehicle jettisons two 70 kg CBMs, offsetting the center of gravity to give the entry vehicle the desired lift-to-drag ratio. This guided entry approach, a departure from the entry styles of the Mars Exploration Rovers (MER) and Mars Pathfinder, results in a reduction of landing error ellipse size and increases the altitude at which parachute deploy occurs.

Entry—During atmospheric entry, entry guidance generates bank angle commands to correct for delivery errors and flight performance. The entry controller translates these commands into commands for the eight entry thrusters. The entry period consists of four parts. First, during entry interface, the attitude is held until the vehicle reports acceleration in excess of 0.2 Earth g's. Second, in the entry guidance range control phase, the bank angle is set to minimize the calculated downrange error at the moment of parachute deploy until the navigated relative velocity is less than 1100 m/s. (Peak heating and peak deceleration occur during the range control phase.) Third, during the entry guidance heading alignment phase, the guidance algorithm minimizes any remaining cross-range error. Finally, the vehicle executes a maneuver called "Straighten Up and Fly Right" (SUFR), ejecting six 25 kg balance masses to set the angle of attack to 0. Parachute deployment is triggered by a range trigger, as opposed to the velocity trigger that was used for the MSL. More information on the range trigger is detailed below.

Parachute Descent—Parachute descent reduces the spacecraft velocity from over approximately 450 m/s to around 100 m/s. Several crucial changes occur during this time. First, the heatshield is separated and the TDS begins acquiring altitude and velocity data relative to the ground. This event utilizes a trigger tuned to initialize separation at Mach 0.8. At 4200 m over the ground, the new LVS (Lander Vision System) starts imaging the ground and providing localization estimates of the vehicle with respect to an onboard map. The best localization solution is input into the new STS (Safe Target Selection) algorithm, which selects the optimal landing site and provides the guidance controller with a guidance target. At 3000 m over the ground, the 8 MLE's are

each commanded to 1% throttle and 8 pyro valves are fired to initiate propellant flow in preparation for powered descent. Backshell separation is then triggered around 2200 m above ground, at a velocity of around 100 m/s.

Throughout the parachute descent, RCS thrusters fire if necessary to counter any wrist mode behavior. A detailed description of this phenomenon is available in [2].

Mars 2020 will be flying a strengthened parachute, a modified version of the heritage design of the MSL's 21.5 m diameter supersonic parachute. This parachute was, in turn, a geometrically scaled version of the 16.15 m Viking-era disk-gap-band design.

Powered Descent— The primary objective of the powered descent phase is to reach the Sky Crane start condition without the risk of any possible collision with the jettisoned backshell and parachute assembly. Following backshell separation, the powered descent vehicle (PDV) experiences freefall to separate its trajectory from that of the backshell. After this, the MLEs throttle up, initiating the powered descent portion. The powered approach trajectory, computed at backshell separation, is designed to eliminate all remaining horizontal velocity and reduce vertical velocity to 20 m/s. It is during the initial stages of Powered Descent that the divert maneuver is performed to target the landing location selected by the LVS. The powered descent segment also includes a sub-segment titled the Constant Velocity Accordion, wherein any accumulated altitude error is flown out. Following this, at an altitude of around 50 m, the constant deceleration segment begins, decelerating the PDV from 20 m/s to 0.75 m/s. At an altitude of 21 m, the PDV throttles down to four MLEs to achieve the required thrust while continuing to operate the MLEs efficiently.

Sky Crane— The Sky Crane start condition is defined at 18.6 m altitude, 0.75 m/s vertical descent velocity, and no horizontal velocity. At this specified condition, the rover is released and lowered from the descent stage to the full length of a triple bridle (7.5 m.) This configuration descends at a rate of 0.75 m/s until touchdown is detected (via the reduction and maintenance of commanded throttle thrust.) While the descent stage and the rover are descending, the rover's mobility system is actively deployed.

Flyaway—After the touchdown detection, the descent stage ceases to descend, severs and retracts the triple bridles, and severs the umbilical. Then, after a brief hold period, the MLEs throttle up and the descent stage climbs and pitches about 45 degrees. This attitude is then maintained, with the MLEs at 100%, expending the remaining fuel supply. At this point, the descent stage follows a ballistic fall to the surface. The end of EDL is defined as the moment when all of the hardware has no kinetic energy relative to the surface.

3. LANDING SITE SELECTION

The Mars 2020 project has followed a similar process to the MSL project in its approach to the deliberation and decision of what is the most appropriate landing site for the given science and mission objectives of the project.

NASA appointed a Mars 2020 Science Definition Team (SDT) in January 2013 to propose objectives and capabilities for the mission. The SDT published a report later that year that included a summary of the potential enhancements
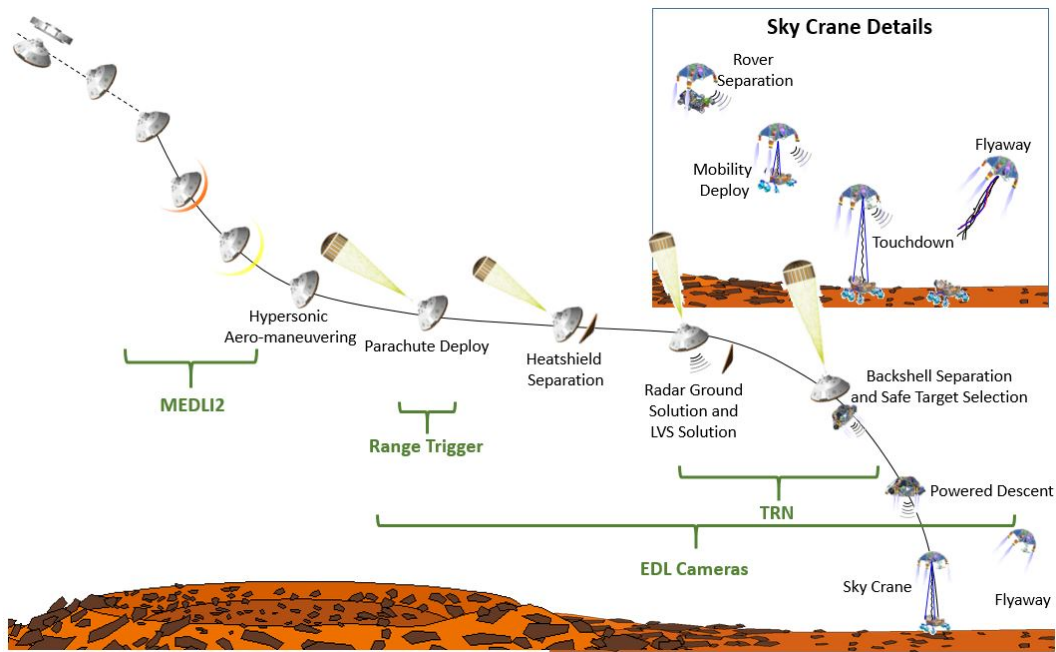
Figure 3. EDL Timeline of Events

to the EDL architecture and how they could improve performance over the MSL, thus providing access to previously unreachable landing sites. The report also provided a summary of landing site engineering constraints, as summarized for the workshops in Table 1. Following the SDT report, the project then embarked on engaging the broader science community through a series of Landing Site Workshops (LSW) where the public was invited to propose or support a particular location through prepared presentations for the community to digest. Typically, the closure of the Workshop has participants grade the sites using criteria that shadows the mission objectives. For each of the workshops, the EDL and Surface teams provided a summary engineering assessment of the sites, to communicate if certain sites presented risks that were unacceptable or out of family with other sites.

Table 1.   Landing Site Engineering Constraints

Landing Site Constraint	Summary Parameter Value
EDL Landing Ellipse Dimensions	25 km x 20 km
EDL, Thermal, Power Latitude Constraint	30 deg N to 30 deg S
EDL Landing Site Elevation	< -1 km relative to Martian datum (effective)
EDL Slope/Roughness	2–10 km < 2 deg, 2–5 m < 15 deg, rocks < 0.55 m
Mobility System Capability (Go to Permitted)	Up to 20 km odometry

The first Landing Site Workshop was held in May 2014. The objectives of this workshop were primarily to establish some leading candidate landing sites that met engineering and planetary protection constraints, and inform the project on how enhanced EDL capabilities could enable those sites specifically.

Based on the outcome of LSW #1, which considered on the

order of 30 sites, the project carried forward nine highly ranked sites for continued engineering analysis. These choices fed specific imaging requests for HiRISE imaging to the Mars Reconnaissance Orbiter (MRO) operations team, as this is our primary source for imaging products used to inform the engineering analysis.

Leading in to LSW #2, the EDL team assessed the validity of the engineering models and system margins for each site to inform the relative risk. This assessment included the evaluation of where TRN was an enabling capability to reach a site with acceptable success probability. One of the sites analyzed was deemed feasible without TRN, and the most highly ranked sites were shown to require the capability. One particular site, Nili Carbonate, was shown to have marginal safety overall. The outcome of this workshop was a set of eight sites recommended for further engineering assessment, informed by the engineering assessment and the desire to carry sites that, collectively, offered broad set of unique scientific units.

LSW #3 was held in in 2017 with the intent of down selecting to a small number of sites in order to focus resources on deepening the understanding of scientific return and engineering performance. Similar to the previous workshop, one site in particular was shown to have lower certainty in the engineering analysis. This site, Southwest Melas, was also not ranked in the top three by the science community and was therefore not carried forward for consideration. The three sites recommended for continued evaluation were: Jezero Crater, NE Syrtis, and Columbia Hills (Gusev Crater).

The locations of the Jezero Crater and NE Syrtis ellipses are approximately 40km apart. Following the conclusion of LSW #3, it was realized that a majority of the scientific targets at NE Syrtis were also available further north, as one moves closer to the Jezero Crater site. This led the science and engineering teams to look for a possible ellipse placement in this region. After initial assessment, a fourth site placed in this location was added for consideration, currently referred

to as Midway.

In October 2018, the project supported the fourth and final landing site workshop. This was the last scheduled opportunity for the public to provide input on the candidate sites prior to the Mars 2020 project making a recommendation and NASA Headquarters declaring the official landing site. On the MSL, the urgency to declare a final landing site months before launch was less pronounced because the project had capability to react to a decision close to, and even after, launch. For Mars 2020, TRN drives requirements for on-board map products that require more time to develop and certify. Hence the desire to select a landing site sooner.

Prior to the final workshop, the EDL team presented their detailed engineering analysis at the Landing Site Safety Assessment review. The review board agreed that the analysis was sufficient in both the quality of imagery and other site-specific products used, and in the team's understanding of the relative engineering performance and risk of each landing site, to support a final landing site selection well ahead of the Mars 2020 launch of July 2020.

The EDL system sensitivities, in general, are very similar to those described in the MSL EDL Overview paper. [2] For Mars 2020, the changes in sensitivity are due to the architecture changes of Range Trigger and TRN. Changes due to Range Trigger are agnostic to site. For TRN, we have the potential to be more sensitive to differential risk as it relates to type and severity of hazard. While the final candidate sites have some unique types of hazards or more prevalence of certain hazards (e.g. sand dunes or rocks), the use of TRN makes the terrain-related success probabilities very similar. Going in to the final workshop, the EDL team was prepared to support the selection of any of the top four candidate sites.

In November 2018, NASA Headquarters followed the recommendation made by the scientific community in LSW #4 by selecting Jezero Crater as the landing site for the Mars 2020 rover.

Landing Site Terrain Characterization

Terrain relative navigation has enabled the selected landing sites, making use of the volume margin in the MSL propulsion tank design. As long as there is a sufficient distribution of safe zones within the landing ellipse, TRN can mitigate terrain-based risks. TRN chooses which point to target based on an onboard safe targets map, which is an expected guidance error buffered version of the hazard map. The hazard map is composed of three main classes of hazards; slope-based, traversal-based, and rock-based hazards. The primary hazard sources used in developing the hazard map are shown below in Figure 4.

Slope-based hazards would risk the rover tipping over or landing the rover with a top-deck angle greater than 30 deg. This angle meshes with the planned limit for traversal testing, allowing buffer in the event that the top-deck angle increases, should the rover need to drive onto a rock to leave the initial landed location. At the time of writing, the team has complete Digital Elevation Model (DEM) coverage at Jezero Crater and uses a roughly 20% buffered ellipse for placement and guiding data acquisition. Data products from the Mars Reconnaissance Orbiter (MRO) allow for the generation of slope data, which facilitates the application of the slope risk mapping generated by ADAMS Monte Carlo work.
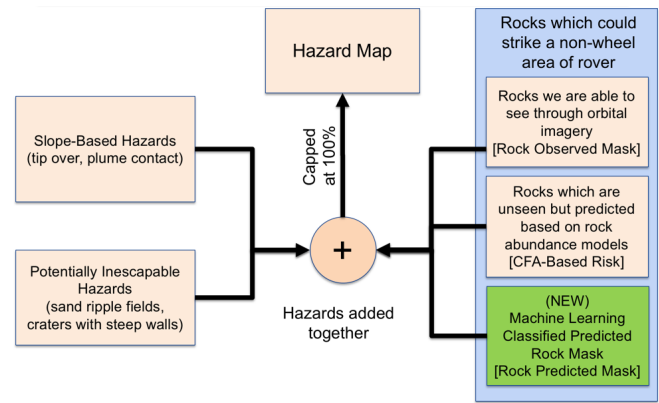

Figure 4. **Terrain hazards included in Hazard Map**

A reevaluation of the traversal hazard type was performed using the MSL driving experience on rippled sand, pictured below in Figure 5. Curiosity's traversal across Dingo Gap raised concerns about ease of travel. Though there was a near flat global slope to the ripple field after Dingo Gap, the rover behaved as if it were driving up a steep sandy slope with 50% wheel slippage. It was determined that the right frequency of sand ripples could present a ripple in front of every wheel at the same time, simulating a climb up highly sloped sand. Later experience on ripples involved two cases of near 80% slip where the rover had to carefully back up and abort traversing through the field.

Areas at the sites with a concerning ripple frequency or a potential for that frequency were treated as inescapable hazards for TRN to avoid, as shown in Figure 6. The time-intensive marking of these hazards was performed by humans stretching the grayscale images to highlight ripple patterns of potential concern. The placement of the rover in an inescapable ripple field is considered an EDL failure. This inescapable hazard map is summed with the slope and rock hazard layers to make the final hazard map.

Figure 5. **Ripple fields encountered by the MSL**

The most abundant hazard type at the selected sites deal with predicted rocks, both seen and unseen. The highest confidence for the predicted models occurs when all rocks between 1.5 - 2.25 m diameter are determined from orbit. The MSL only ever had the results from a single image used to cover the areas within the ellipse. With highly accurate tiepointing, Mars 2020 is able to combine rock detections from multiple overlapping images to create a large composite rock field in lat / long space. Consistency of rock cumulative fractional area (CFA) estimates across the ellipse and across areas of different degrees suggests the rocks with the diameter
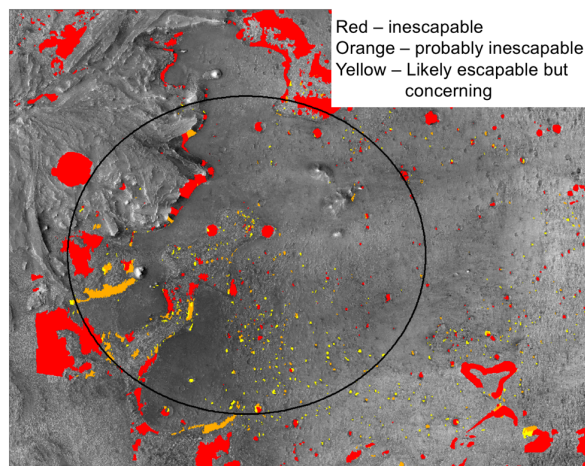
Red – inescapable
Orange – probably inescapable
Yellow – Likely escapable but
concerning

Figure 6. **Inescapable hazard characterization for Jezero candidate landing site**

window used for CFA estimation (i.e. 1.5 - 2.25 m diameter) are sufficiently characterized. The lower bound is roughly 5 pixels in a HiRISE image. Typically, a success rate of 85% in determining rocks with 5 pixel shadows or greater can be expected; based off of Mars Analog testing. [6] Combining multiple images allows the opportunity for higher percentages, as shown in Figure 7.
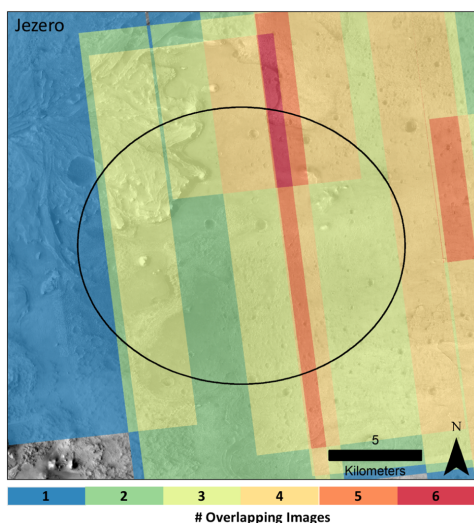

Figure 7. **Overlapping HiRise images improves rock identification success percentage**

The red dots shown in Figure 8 are each a Machine classified rock, based from shadow detection, and a Machine Learning convolutional network classification of each pixel. Every rock observed from orbit or predicted using Machine Learning has been classified as a death hazard for these initial assessments of landed risk. The final hazard maps will use these assessments as an initial baseline, to then be refined based on human marking.

The number of measured rocks between 1.5 and 2.25 m diameter fit a specific rock CFA curve. With overlap, it is highly likely that all rocks >1.5 m diameter are seen. Rocks over 2.25 m diameter are trimmed as any false positive detections could strongly mislead the CFA curve fit (though these rocks are uncommon.) The CFA is used to estimate the

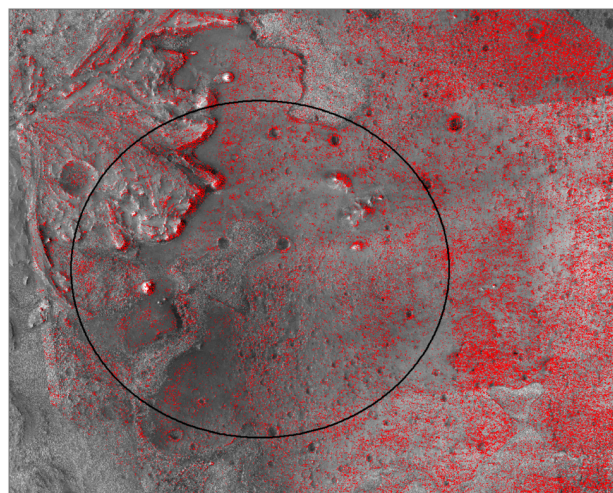risk of rocks <1.5 m diameter that are unseen from orbit.

Figure 8. **Red dots denote rocks identified at Jezero candidate landing site using Machine Learning techniques**

Mars 2020 uses a moving circular kernel to calculate CFA locally. The calculation is performed and the result is placed into the 10x10 m cell in the middle of the circle. The circular kernel is then moved 10 m and the calculation is redone. This creates a CFA with far more reasonable locality information than the square kernel used by the MSL without any computational overlap.

All hazard types including slope, traversal, and rock-based layers are then combined and capped at 100% death. Regions without significant data are tracked as 100% death. This is the final hazard map used to evaluate the success of a landing simulation and a buffered form is carried onboard as the Safe Targets Map utilized by TRN. Shown in Figure 9, the hazard map is the combination of an effort to correctly characterize the terrain and the mapping between terrain and risk to the system.
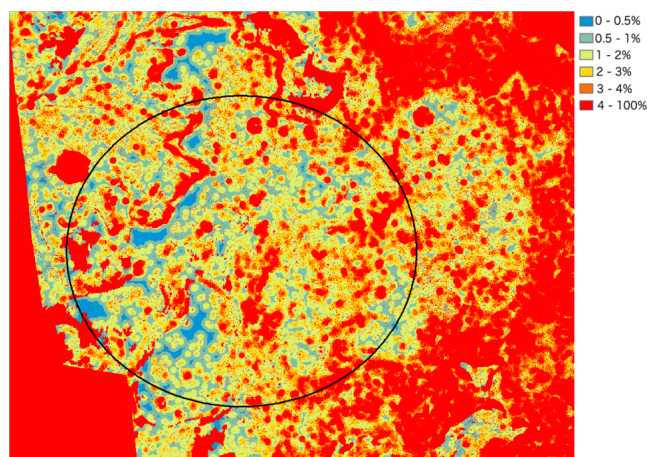

Figure 9. **Example hazard map for the Jezero candidate landing site**

4. LESSONS LEARNED SINCE THE MSL

Touchdown Velocity

The MSL experienced a lower than expected touchdown velocity, spawning investigations into the effects of the sandy radar phenomenon, as well as efforts to implement site-specific gravity modeling on M2020.

Sandy Radar— In flight, the Mars Science Laboratory observed errors in radar line-of-sight velocity measurements. These errors were more frequent as the vehicle descended during the Sky Crane maneuver, though they were infrequent enough so as to not significantly skew the ensemble of radar measurements.
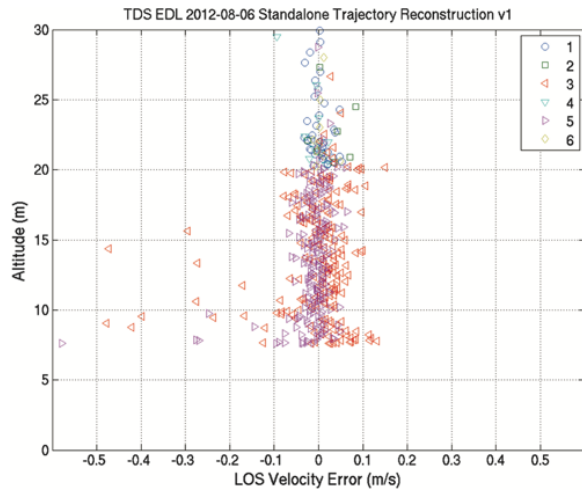

Figure 10. **Plot of altitude vs. radar beam line of sight velocity error for measurements just before and during Sky Crane.**
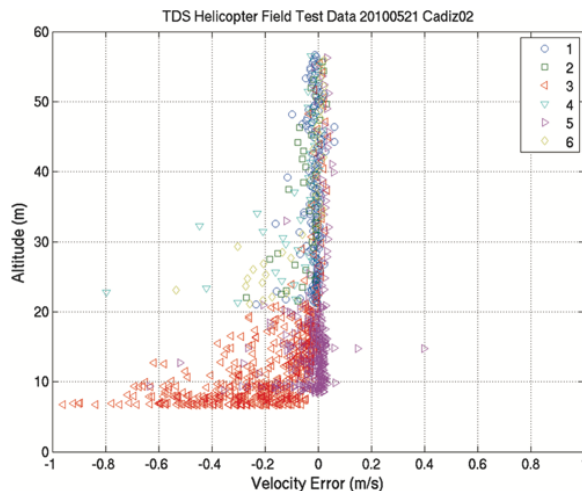

Figure 11. **Plot of altitude vs. radar beam line of sight velocity error for measurements from a TDS engineering model during a helicopter test over Cadiz Dunes.**

The most likely cause of the errors is the motion of surface material excited by the plumes of the Descent Stage's Mars Landing Engines (MLEs).[7] This explanation is supported by the resemblance between the characteristics of the errors and those of similar errors seen during Earth-based helicopter

testing of the TDS engineering model, as shown in Figures 10 and 11. The fact that significant amounts of dust and debris were kicked up by the MLEs is confirmed by Mars Descent Imager (MARDI) images collected during EDL (Figure 12).
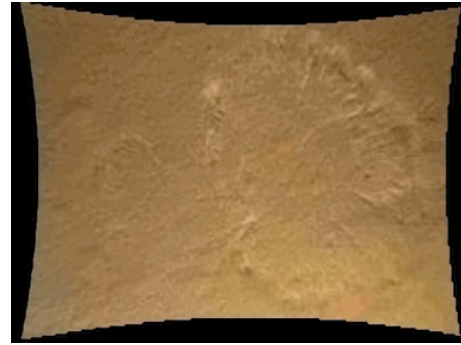

Figure 12. **MARDI image showing plume induced motion of ground material at the time of Sky Crane.**

For Mars 2020, radar behavioral models in end-to-end EDL simulations have been augmented to capture the potential effects of plume-induced velocity errors. Previously on the MSL, these models had only been used in standalone stress and robustness analyses. The models, which were intended to conservatively bound this effect, have been tuned to further bound the MSL inflight data. The model is now used in all performance analyses, resulting in higher touchdown velocity ranges. Even with increased touchdown velocity errors, the system is still within the rover's touchdown capabilities and requirements.

Site-Specific Gravity Modeling— The MSL experienced a lower than expected touchdown velocity, an anomaly slated to be corrected for M2020. Inaccurate altitude and velocity estimates during the Sky Crane maneuver resulted in an observed touchdown velocity outside the 3-sigma predictions (0.63 m/s vs 0.75 $\pm$ 0.1 m/s vertical, 0.18 m/s vs 0$\pm$ 0.11 m/s horizontal). The error in the vertical velocity was attributed to an approximately 4.4 mm/s^2 difference between the onboard gravity assumption and the local gravity. (The MSL did not use the TDS to directly measure vertical velocity during touchdown due to spoofing concerns surrounding the possibility of sandy radar.) The error in the horizontal velocity was attributed both to local gravity contamination and the effects of sandy radar. Furthermore, the MSL simulations did not take into account modeling uncertainty with respect to gravity, which presumably would have revealed a touchdown velocity sensitivity to this error term.

Several options were considered to address this anomaly on M2020, with the implementation of a gravity model as the emerging solution. A site specific gravity parameter, based on terrain implied gravity, has been incorporated into FSW, which assumes a J2 model. This delta parameter value captures the difference between the J2 model and the higher-fidelity delivered gravity model. The simulations will include the higher-fidelity Mars gravity model information, including an uncertainty dispersion informed by an error analysis.

The new model, shown in Figure 13, was developed by JPL, using MRO120d data from 3240 km and above.[8] Below this altitude, a new terrain-implied gravity model was developed. The model can be queried at the surface at all possible landing sites, providing a correction term to the FSW.
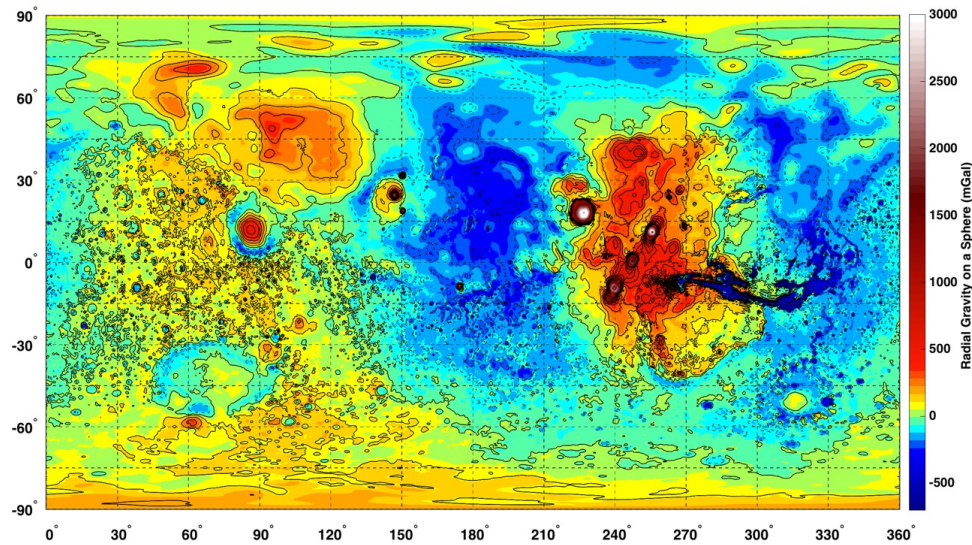
Figure 13. **Mars 2020 High Resolution Gravity Model.**

ASPIRE Test Campaign

The failure of two supersonic parachutes that were tested as part of the Low-Density Supersonic Decelerators (LDSD) project led to a number of inquiries into our understanding of supersonic parachutes. Although the configurations tested by LDSD were not Disk-Gap-Band parachutes that are typically used at Mars, the design tools, test techniques, and overall test paradigm were similar. Through a series of studies and reviews, two basic premises emerged related to the supersonic parachute design and test paradigm and how our recent DGB parachute designs have compared to the historical precedent. Prior to LDSD, there was a belief that a subsonic parachute inflation adequately recreated the stresses and loads that a parachute would see during a supersonic inflation. More careful study of the supersonic inflation process, facilitated with data from LDSD, indicated that was not likely the case. In particular, the speed and asymmetry associated with a supersonic inflation can lead to stresses that are higher in magnitude and in locations that otherwise would not be achieved in a subsonic inflation. A review of historical DGB designs [9] also pointed to a trend in the theoretical capability of recent DGB designs relative to the loads that they ultimately were tested or flown at. Particularly in the case of the MSL, the theoretical capability of the parachute was much closer to the as-flown load than prior parachutes that had been used successfully at Mars.

Based on the above, M2020 undertook two separate activities, the design of a strengthened version of the MSL DGB parachute and a risk-reduction activity to supersonically test the parachute. [10] From the latter, the Advanced Supersonic Parachute Inflation Research Experiments (ASPIRE) project was created. ASPIRE utilizes a two-stage sounding rocket to carry a payload to altitudes and velocities that simulate the conditions for an inflation at Mars. An overview of the ASPIRE flight sequence is shown in Figure 14, with the values shown corresponding to the conditions for the 3rd ASPIRE flight (SR03). The sounding rocket assembly, consisting of a Terrier first stage, a Black Brant second stage, and the roughly 1200 kg payload section containing the parachute, are launched out of NASA's Wallops Flight

Facility (WFF). The system is rail-launched and spin-stabilized at 3.5 Hz. During a flight, the first and second stages burn out and the payload section reaches apogee between 45 km and 55 km. When the payload reaches the target dynamic pressure (q_∞) and Mach number conditions, the parachute is mortar-deployed. The deployment, inflation, and supersonic and subsonic aerodynamics of the parachute are analyzed by a suite of instruments including: a three-camera high- speed/high-resolution stereographic video system trained on the parachute, situational awareness video cameras, a set of load pins at the interface of the parachute triple-bridle and the payload, and a GPS and inertial measurement unit (IMU) onboard the payload. After decelerating to subsonic speed, the parachute and payload descend to the Atlantic ocean for recovery, return, and detailed inspection.

The original ASPIRE test matrix was focused on at least four flights with the first testing a build-to-print version of the MSL canopy and the later three testing a strengthened parachute. A higher than anticipated load on the second flight allowed for the test matrix to be compressed to only three flights total. Additional details of those are available in References [11] and [12].

A summary of the test conditions and measured tension loads from the three flights are presented in Table 2 and Figure 15. Overall, all three flights were very successful and the last two flights pushed the strengthened parachute to inflation loads significantly higher than those anticipated by M2020 at Mars. Each parachute was recovered from the Atlantic Ocean and inspected for damage. Although some small damage was observed and attributed to deployment, none of the damage was cause for concern. After the conclusion of SR03, the project concluded that ASPIRE had sufficiently reduced the residual risk of supersonic parachute inflation for M2020 to proceed to Mars with the strengthened parachute design.

Parachute-IMU Interactions

The anomalies reported by the European Schiaparelli lander led to a reexamination of potential ways in which M2020
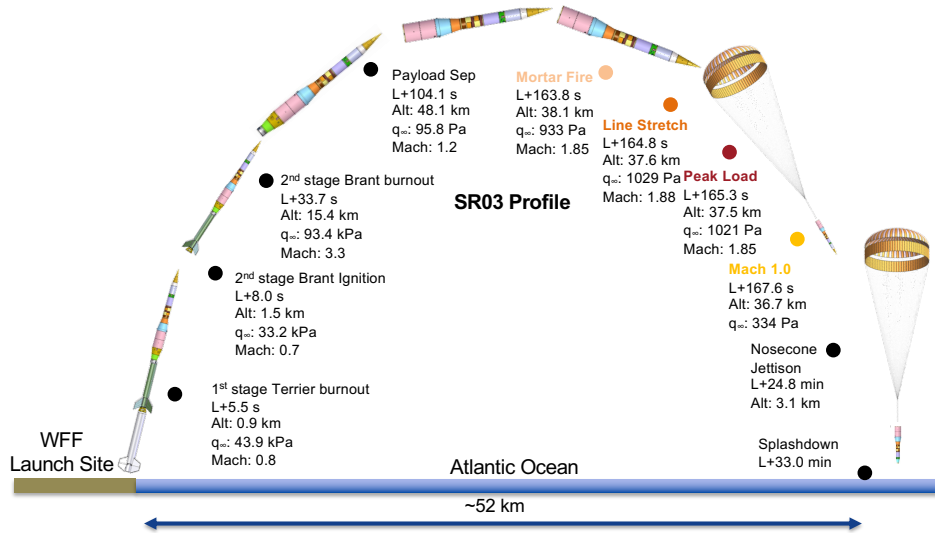
8

Figure 14. **ASPIRE Test Profile for SR03**

Table 2. **Summary of ASPIRE Test Conditions**

|		Mortar Fire	Line Stretch	Peak Load	2nd Peak	Mach 1.4	Mach 1.0	Mach 0.5
Time From Launch (sec)	SR01	161.411	162.372	162.878	163.087	164.359	167.016	179.634
	SR02	177.588	178.626	179.081	179.273	180.719	182.865	193.431
	SR03	163.820	164.847	165.257	165.460	166.150	167.587	174.627
Mach	SR01	1.77	1.79	1.77	1.71	1.40	1.00	0.50
	SR02	1.97	2.00	1.97	1.89	1.40	1.00	0.50
	SR03	1.85	1.88	1.85	1.73	1.40	1.00	0.50
Dynamic Pressure (Pa)	SR01	452.4	491.7	494.7	466.3	332.1	188.1	64.3
	SR02	670.6	744.6	746.5	694.7	416.5	233.1	76.9
	SR03	931.7	1028.4	1020.1	909.6	615.5	333.6	99.8
Geodetic Altitude (km)	SR01	42.4	42.0	41.8	41.7	41.3	40.5	38.2
	SR02	40.8	40.3	40.0	39.9	39.3	38.6	36.6
	SR03	38.1	37.6	37.5	37.4	37.1	36.7	35.4
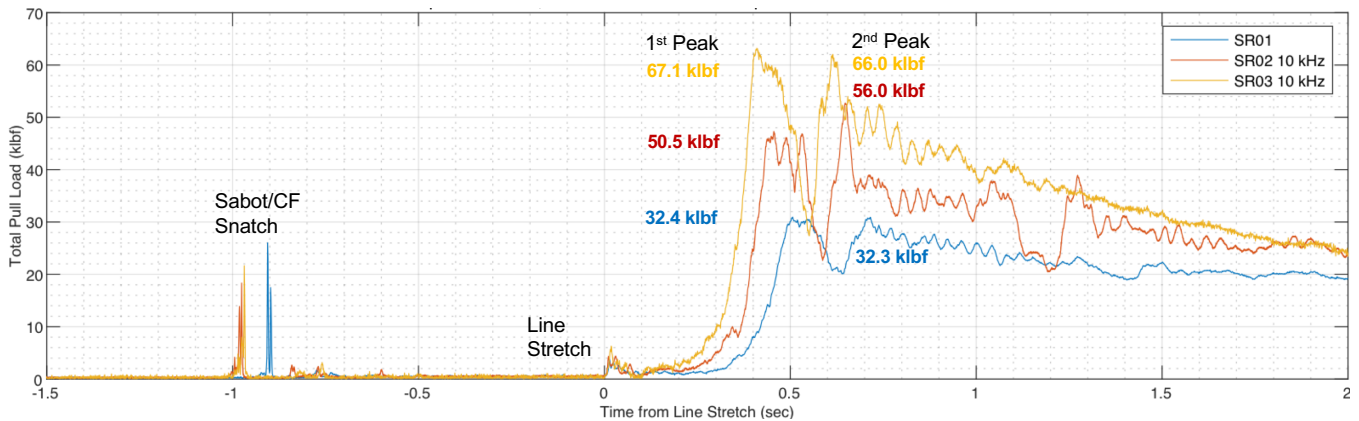
Figure 15. **Measured inflation pull loads for each of the three ASPIRE flights. Note that the bold numbers are for total parachute force which accounts for the mass of the parachute and high deceleration environment.**
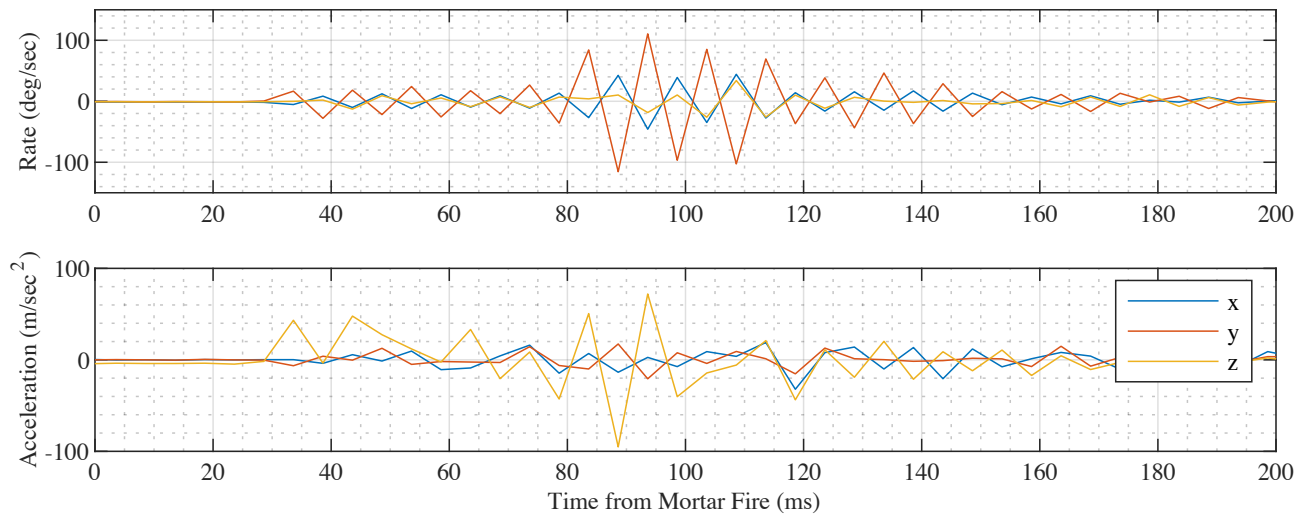
9

Figure 16. **Measured rates and accelerations during the very beginning of the MSL parachute deployment**

could saturate the Descent Inertial Measurement Unit (DIMU). One area of concern was associated with the reaction loads from the parachute mortar, which would need to increase with the use of the heavier strengthened parachute. A review of the 200 Hz data from the MSL entry revealed unexpectedly high attitude rates and accelerations around the time of parachute deployment. Shown in Figure 16 above were the measured rates and accelerations from the MSL within the first 200 ms after mortar fire. Of note is that the disturbance does not appear until about 80 ms after the mortar fire command is sent. Correlating this timing with data from the MSL mortar development program, it was determined that the disturbance was most likely due to two snatch events that occurred around that time, that of the sabot and of the confluence fitting. The parachute sabot is a 5.2 kg piston that pushes the parachute pack out of the mortar can and the confluence fitting is a 3.7 kg titanium link between the triple bridle and parachute riser. Both are ejected out of the mortar can at between 40 and 45 m/sec and must be arrested. In both cases, the load paths were through the very stiff Kevlar bridle legs. A quick hand calculation estimated that the snatch loads in both cases could exceed 100 klbf, much more than was thought possible during the MSL development.

The MSL DIMU reported an oscillation of ~100 Hz with a peak of 120 deg/s. However, because the raw gyro data is sampled at 200 Hz, the 100 Hz oscillation is likely aliased and it is not possible to know how high the peak value truly was. Further examination pointed to a likely mechanism of the high rates being the excitation of the DIMU due to the rapid, less than ~5 ms, snatch events associated with the sabot and confluence fitting. The impulse from these two snatch events likely excited a local mode on the panel that the DIMU was mounted to. Although the DIMU also utilizes internal isolators, they were noted to have frequencies similar to the modal frequencies of the DIMU panel, thus leading to amplification from the panel.

Mars 2020 utilizes the same DIMU as the MSL and there was concern that the disturbances from the two snatch events could lead to saturation of the DIMU. If the DIMU [13] were to saturate, a loss or significant degradation of attitude knowledge could follow and lead to a potential loss of mission. To address the concern, M2020 implemented a number of mechanical changes to the parachute system and

is presently investigating a range of potential changes on the GNC side as well. On the mechanical side, the load path associated with the sabot snatch was decoupled from the triple bridles and instead rerouted through tapes that are part of the sabot capture net. The tapes themselves were changed from the Kevlar that was used on the MSL to a Nylon tape. Additionally, the bridles themselves were changed to Nylon, which reduced the stiffness of the bridle legs by a factor of 20. Lastly, the confluence fitting was reduced in mass to approximately 3 kg. Combined, these changes are expected to reduce the magnitude of the disturbances significantly. The effects of these changes will be confirmed through mortar testing.

On the GNC side, multiple options are being considered. Modifying the output resolution of DIMU from 1 μrad to 5 μrad would increase the saturation limit five fold. Another option that is under consideration is using the IMU in the Rover as another source of data during parachute deploy.

Radiative Heating Effects

The Mars 2020 Thermal Protection System (TPS) will be nearly identical to that of the MSL, using the same materials and thicknesses. The most important changes to the Mars 2020 aerothermal environments analysis are a new design trajectory for the Mars 2020 arrival period and the addition of shock layer radiation to the total heat transfer. Testing and analysis since the MSL launch, plus indirect clues from MEDLI heatshield instrumentation, require the addition of radiative heat transfer to all regions of the Mars 2020 aeroshell. This change required TPS thermal response sizing analysis at many more body points than were used for the MSL. Radiation contributes more than convection to the total heat transfer for many parts of the Mars 2020 aftbody, especially the Backshell Interface Plate (BIP) and Parachute Closeout Cone (PCC). The MSL TPS was sized to conservative convective heating only, often utilizing the worst-case heating calculated anywhere on an aftbody component (backshell, BIP, PCC, or PCC lid) placed on the location with the lowest thermal mass. In some cases, like the PCC lee-side cone and lid, the MSL used the worst-case PCC wind-side convective heating with a multiplying factor (0.5 for the PCC lee side and 1.75 for the PCC lid). Mars 2020 analyses took care to combine convective and radiative
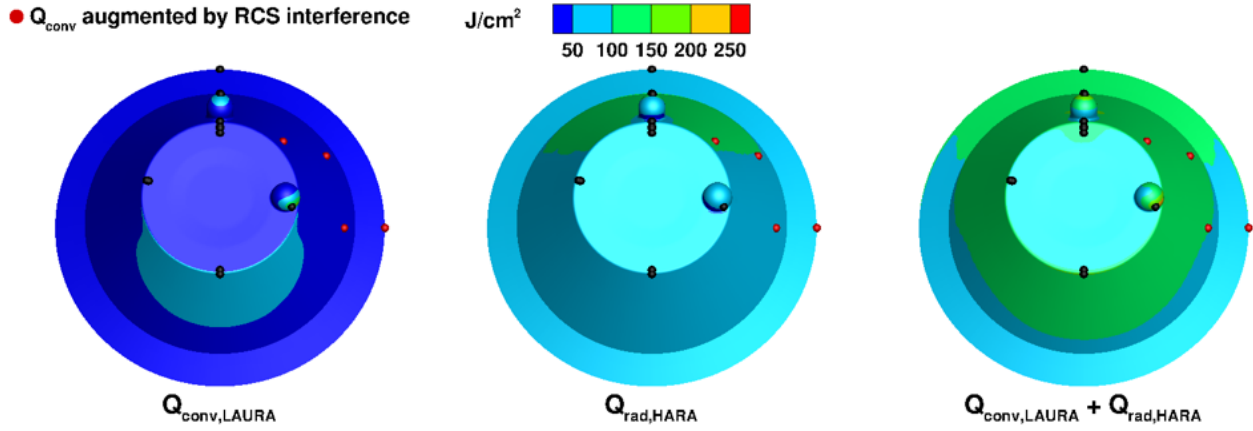
Figure 17. **Integrated heat load (convective from LAURA on the left, radiative from HARA in the middle, and combined on the right), with uncertainties, on the BIP and PCC.**

heating and the actual structure for each of the aftbody components to perform TPS sizing. Figure 17 shows the integrated heat load (convective, radiative, and combined), with uncertainties, on the BIP and PCC. Convective-only heating environments would lead to the selection of TPS sizing locations on the windside PCC cone (lower half) and protuberances. The addition of radiation unveils additional areas of higher heating on the PCC lid and remaining PCC cone and leeside BIP (upper half). Even with the additional heating from radiation, all aftbody components can be built with the same TPS thicknesses that were used for the MSL.

5. New Features and Capabilities

Terrain Relative Navigation

The Terrain Relative Navigation (TRN) system is an enabling Entry, Descent, and Landing (EDL) technology slated for inclusion in the Mars 2020 mission.[14] Past missions have disqualified scientifically compelling landing sites due to hazardous terrain present within the landing ellipse. TRN enables access to previously inaccessible landing sites by mitigating the risk of terrain-related failure. In practical terms, TRN allows hazards up to 200 m in diameter to be present in the landing ellipse as long as they are surrounded by 120 m safe zones; previous missions allowed no significant, contiguous hazardous areas within their landing ellipses. Relaxing engineering constraints placed on the landing site selection process for Mars 2020 has encouraged the planetary science community to consider sites suited for sample collection that were deemed too dangerous for earlier missions.

As shown in Figure 18, TRN is a two-step process: the first step is determining the current position of the spacecraft with respect to the terrain during parachute descent; the second step is using this information to direct its powered descent flight path to a safe landing target. The first step is accomplished by the Lander Vision System (LVS) sensor and the second by the Safe Target Selection (STS) algorithm.

The LVS generates a map-relative localization solution by fusing measurements from a visible-wavelength camera and an inertial measurement unit using the Map Relative Localization algorithms operating on a high-performance compute element. The dynamic state estimate of M2020's heritage EDL system is initialized just prior to atmospheric entry using a stellar reference for attitude and ground navigation for position and velocity; from that point, onboard navigation solutions are propagated using an IMU. The LVS is initialized with the spacecraft's state estimate once heatshield separation has occurred and measurements from the landing radar have been used to correct accumulated velocity and altitude errors. Horizontal position uncertainty can be as large as 3.2 km when the vehicle reaches 4.2 km above ground level (AGL), where a two-phase map relative localization process begins. During the coarse phase, five large patches in each of three images are matched to a coarse onboard map (12 m/pixel). Images are taken slightly slower than once per second. A batch filter computes a correction to the spacecraft's initialization, which is then used to crop a fine map (6 m/pixel, 6 km square). During the fine phase, up to 150 landmarks are matched from each image to the fine map. These landmarks are used as inputs for an Extended Kalman Filter (EKF) that estimates position, velocity, attitude, and IMU biases. The EKF propagates this solution at a rate of 64 Hz and images are taken at a rate slightly greater than once per second. The fine phase achieves a map relative localization accuracy better than 40 m after matching landmarks from three images, which should occur well within the LVS's 10-second allocation to generate a solution. Solutions are sent from the LVS to the primary flight computer at 8 Hz. This phase continues uninterrupted until 2.0 km AGL or until the number of available landmarks drops below 25.

Once LVS has successfully generated a localization solution, the STS algorithm uses this information to find the best reachable safe landing target. This algorithm is an augmentation to the heritage EDL GNC flight software. At the time of backshell separation, STS uses the best available localization solution from the LVS to determine the reachable set of landing points. This set is constructed using parameters tuned according to key system performance metrics, including available fuel, maximum allowed off-nadir angle of the powered descent vehicle, and risk of recontact with the backshell. These points take the form of two wedges, one to each side of the flight path when projected on the terrain. The points from both wedges are searched within the onboard Safe Targets Map (STM) and the safest point from each wedge is saved. Upon comparing these points to one another, STS generates a guidance target and provides it to the heritage powered descent guidance controller.
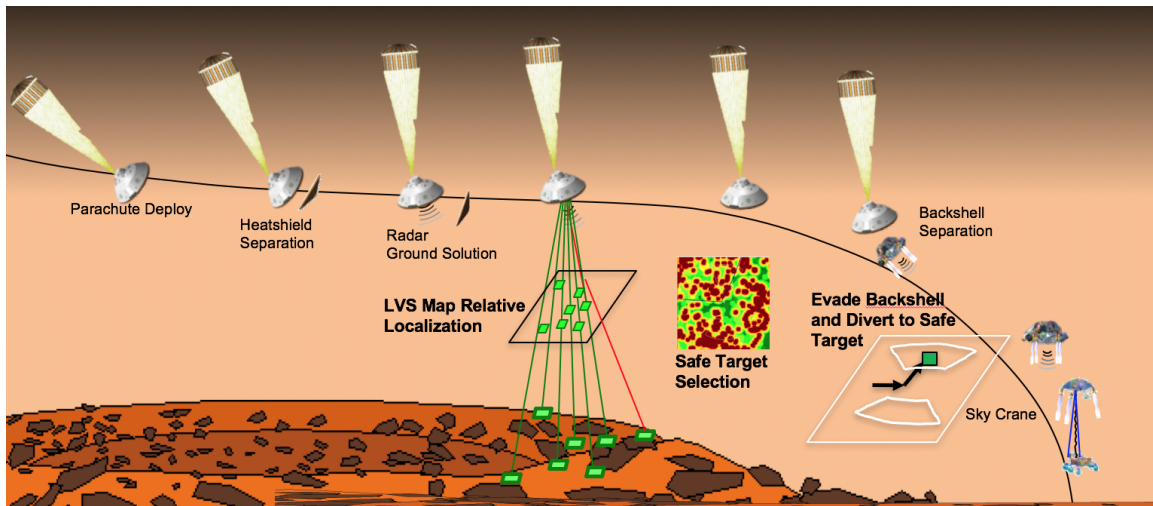
Figure 18. **Key Terrain Relative Navigation events in EDL Timeline**

The architecture of the heritage EDL system is such that few significant changes were required to accommodate TRN. A margin period exists within the EDL timeline where radar-based navigation solutions are already in use but the system is waiting to prime the landing engines at 3.0 km AGL. To support a 10-second period for LVS to generate a localization solution, some of this margin was allocated to guarantee a radar solution by 4.2 km AGL for LVS initialization. To allow for avoidance of large hazards, the backshell avoidance divert was extended from a fixed distance of 300 m to a range of between 300 m and 635 m. Further, instead of a fixed azimuth relative to initial flight path, the backshell avoidance divert azimuth can now be +/- 25 degrees. To accommodate the extended divert, target backshell separation altitude was raised from 1.6 km AGL to 2.2 km AGL. Fuel margin has also been consumed to support the divert maneuver.

The design of the LVS sensor has been evolving for some time. Research and development in this area culminated in the implementation of the same core MRL algorithms in the LVS as part of a prototype sensor package. This prototype system also shared many architectural details with the current implementation of the flight build. The prototype system was demonstrated in 2014 in a series of field tests over Mars-analog terrain in Death Valley and the Mojave Desert, proving the capability to generate a localization solution with better-than-40 m accuracy within 10 seconds of initialization. Performing the image processing for the coarse and fine phases, running the batch filter and EKF, and propagating solutions with IMU data is a set of tasks not suited for a standard flight processor. The LVS sensor has two parts: a Vision Compute Element (VCE) and a LVS Camera (LCAM). The VCE has been specifically developed to handle this processing. The VCE is composed of a MSL-heritage power conditioning card, an off-the-shelf BAE RAD750 flight computer, and a new Computer Vision Accelerator Card (CVAC). The RAD750 functions as the sensor's executive and runs the VCE flight software. The CVAC contains two FPGAs, all of the VCE's data interfaces, and most of its memory. The CVAC's Vision Processor (VP) FPGA is a reprogrammable Xilinx Virtex5 that handles computationally intensive image processing tasks and allows LVS to meet its timing requirements. The CVAC's Housekeeping (HK) FPGA is a burn-once RTAX 2000 that handles time synchronization, power management, ADC, and other interfaces. Imagery is gathered by a dedicated LVS Camera (LCAM), which is powered and managed by the VCE. Completing the sensor package is data from the Descent IMU (DIMU). DIMU data is shared between M2020's primary flight computer and the VCE via a Y-split cabling configuration.

TRN is a robust capability that has dramatically altered the available set of landing sites to Mars 2020 and future EDL missions. Overall probability of success figures for the selected Mars 2020 landing site increase from below 90% to around 99% after considering the impact of TRN.

Range Trigger

In the Viking-heritage EDL system at Mars, the first vehicle configuration transition that must be performed is the deployment of a parachute. At Mars, the low atmospheric density, and consequently high terminal velocity of the entry aeroshell, necessitates that this transition be performed supersonically and at modest dynamic pressures. These conditions result in a challenging deployment, very rapid inflations, and high opening loads and stresses in lightweight fabrics. Additionally, the two orders of magnitude difference in density between Earth and Mars makes testing and verification of the system both difficult and expensive, thus limiting the opportunities to study and drive-down the risks. As a result, it is absolutely crucial that the EDL system autonomously deploys the parachute within a relatively narrow window, defined by previous qualification programs. For Mars 2020, this window is defined by the Viking qualification box of: $1.1 < M < 2.2$, $239 < q < 850\ Pa$ and a Flight Limit Load (FLL) of $50,000\ lbs$[2].

The original design of the Apollo-derived entry guidance for the MSL called for this event to be triggered by an on-board guidance estimate of the range to go to the target[15]. This range trigger, sometimes referred to as "Smart Chute", was eventually replaced by a planet-relative velocity trigger in order to minimize the risk of deploying above the upper constraint on Mach number, while attempting to maximize the landing site elevation capability of the system in the face of developmental mass growth. It is important to note that due to the lateness of the landing site selection, this

---

[2]This FLL was reduced from that of the MSL $65,000\ lbs$ in order to improve safety factors in the parachute qualification program.
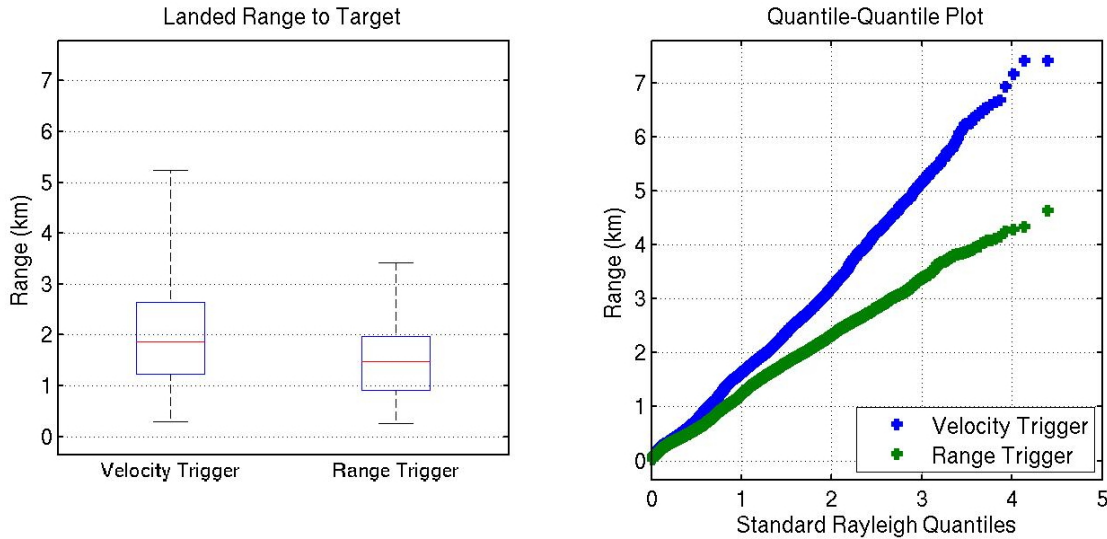
Figure 19. **The effect of trigger type on statistics for landed range to target. The figure on the left compares these data using a box-and-whiskers format. In this figure, the box depicts the middle 50 percentile, the whiskers indicate the 1 and 99 percentile, and the red line in the center of box shows the median value. The figure on the right presents the same data in a quantile-quantile plot. In this plot, the quantiles of the data are plotted against equivalent quantiles of a standard Rayleigh distribution.**

decision needed to be made well before the final landing site, Gale Crater, was selected. The low elevation of Gale, -4.5 km below the reference datum, allowed for a much less aggressive target Mach number of 1.7, alleviating the original concerns that drove this design decision.

In theory, any parameter or combination of parameters, which are estimated on-board, may be used within the flight software logic to trigger the mortar fire event, and will perform identically in a nominal sense, without regard to uncertainties. In practice however, the performance of any given trigger, in light of uncertainties, and with respect to the parameters it does not control, introduces a very detailed and nuanced evaluation of the relative risks involved. For a velocity trigger, dispersions in velocity are minimized by design, but this trigger results in larger landing footprints. Conversely, a range trigger minimizes downrange dispersions, and thus footprint size, though at the expense of larger velocity dispersions. Way [16] provides a detailed side-by-side comparison of range and velocity triggers and describes a wind correlation that minimizes Mach number spread in the case of a range trigger, in spite of the increased spread in relative velocity. The actual magnitude of the footprint reduction is unique to each situation, and depends on the relative contributions of other modeled dispersions [17].

Given the particular characteristics of the considered landing sites, the Mars 2020 project has adopted a range trigger for the activation of the Straighten-Up and Flight Right (SUFR) maneuver, in lieu of the MSL-heritage velocity trigger. Though trivial to implement in the flight software – effectively changing only a single line of code – this change significantly reduces the size of the expected landing ellipse. Relatedly, but for an independent reason, the mortar-fire event is now initiated on time (a fixed 17 seconds following SUFR), rather than on an additional velocity trigger. This design alleviates any concerns of a possible collision[3] between the

two triggers.

Table 3. **Footprint Comparison**

Parameter	Range Trigger	Velocity Trigger	Difference
Major Axis, km ($2a$)	7.11	11.10	-35.9%
Minor Axis, km ($2b$)	6.53	6.37	+2.5%
Area, km^2 (πab)	36.48	55.55	-34.3%

Table 3 compares 99 percentile footprints for the Mars 2020 mission. The minor axis, which is oriented in the cross-track direction, is nearly the same for both footprints. This is expected, since the cross-track performance is unaltered by downrange targeting. The major axis, however, oriented along the down-track direction, shows a nearly 36% reduction when using the range trigger. Combined, this results in a nearly 35% reduction in landing footprint area. Figure 20 and 21 show the landing footprints for the velocity and range trigger, respectively. The difference is notable. In addition, Figure 19 compares the statistics for the expected miss distance (landed range to target) and shows a nearly 2 km reduction in the 99%-tile.

Importantly for the mission, this reduction in footprint size is significant when positioning the ellipse in the vicinity of hazardous terrain.

MEDLI2

Mars Entry, Descent, and Landing Instrumentation 2 (MEDLI2) is a suite of sensors located on the Mars 2020 heatshield and backshell, which will measure pressure, temperature, and heat flux during the entry phase of the mission.[18] These measurements are used for post-flight reconstruction of the aerodynamic and aerothermal environments seen during EDL, as well as to better constrain thermal protection system (TPS) margins. The

[3]For the MSL, since both events were triggered on velocity, a higher than

expected deceleration could reduce the actual time between the events below the minimum required time to finish the EBMD balance mass ejections.
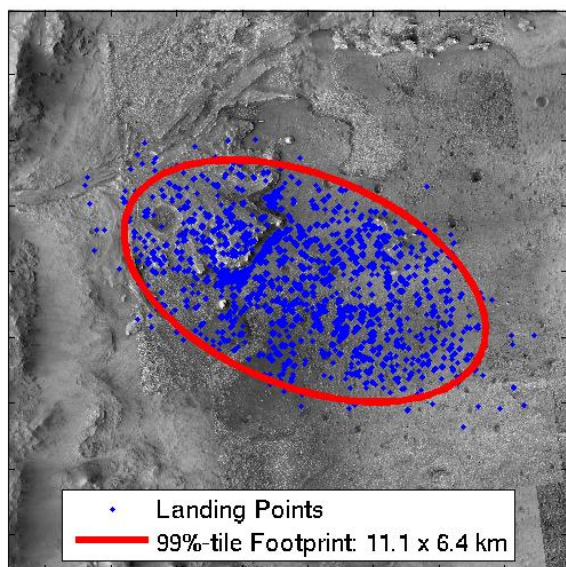
Figure 20. **Velocity trigger footprint. This figure depicts 8000 Monte Carlo landing points at the Jezero crater landing site, along with a 99%-tile ellipse. The size of this ellipse is 11.1 x 6.4** km**.**
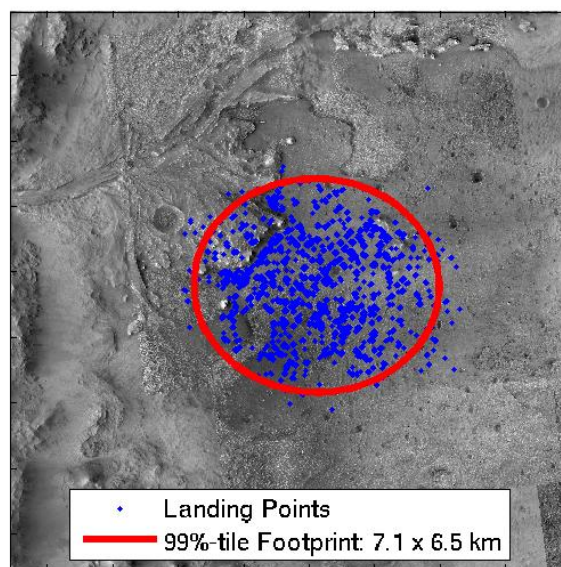

Figure 21. **Range trigger footprint. This figure depicts 8000 Monte Carlo landing points at the Jezero crater landing site, along with a 99%-tile ellipse. The size of this ellipse is 7.1 x 6.5** km**.**

instrument suite is divided into three subsystems: the Mars Entry Atmospheric Data System (MEADS), the MEDLI2 Integrated Sensor Plugs (MISP), and the Sensor Support Electronics (SSE). MEADS consists of pressure transducers attached to the inner mold line of the aeroshell and connected to flush orifices in aeroshell TPS materials. The MISP subsystem consists of heat flux sensors and thermocouples embedded in the TPS materials. The SSE serves as the interface between MISP and MEADS sensors and the Mars 2020 flight system, energizing the sensor hardware and relaying data to the spacecraft. Figure 22 shows these MEDLI2 hardware elements and their general locations on the Mars 2020 aeroshell.

MEDLI2 will add to the dataset that was started by the original MEDLI on the MSL, which instrumented the heatshield portion only of the aeroshell with pressure and temperature sensors. [19] [20] MEDLI transducers were designed to measure the entire pressure range during entry between 0 and 35,000 Pa. A key finding from this experiment on the MSL was that the hypersonic pressure transducers were not sufficiently accurate at supersonic flight conditions. To improve the dataset's accuracy in supersonic conditions, MEDLI2 will carry six transducers tuned for the 0 to 7,000 Pa pressure range. A seventh transducer, a flight spare from MEDLI, is included in MEDLI2 to measure the hypersonic stagnation pressure. The locations of pressure transducers on the heatshield were determined using an optimization algorithm to minimize errors in reconstructing the vehicle angle-of-attack and side-slip angle. The MEDLI2 MISP design for the heatshield prioritizes near-surface temperature measurements, with an increased number of TPS plugs containing near-surface thermocouples distributed over the heatshield. Temperature measurements from these sensors will better capture the transition to turbulence and identify the turbulent footprint on the heatshield. Three Thermal Response plugs are also included, which contain three thermocouples set at different depths within the TPS plugs, allowing the in-depth response of the TPS material to be measured. Heatshield

TPS plugs containing thermocouples are manufactured from the heatshield TPS, Phenolic Impregnated Carbon Ablator (PICA).

Another noteworthy addition for MEDLI2 is the inclusion of backshell instrumentation, which consists of one pressure transducer, six TPS plugs instrumented with thermocouples, two total heat flux sensors, and one radiative heat flux sensor. The pressure transducer is tuned for the very low pressures expected on the aftbody, ranging from 0 to 700 Pa. Thermocouples embedded in TPS plugs filled with the backshell TPS, SLA-561V, will characterize the aerothermal environment in the attached and separated flow regions of the backshell. Additionally, relatively low heat rates of less than 25 W on the backshell enable the use of sensors designed to make direct measurement of heat flux. Therefore, the MEDLI2 backshell sensor suite includes three embedded heat flux sensors. One of these sensors will use a sapphire window to prevent airflow, allowing it to measure only the radiative component of the total heat flux. This is an important measurement, because radiative heating has been identified as a significant contributor to the total heat flux seen by the vehicle aftbody.

EDL Cameras

While extensive reconstruction of the entire EDL sequence can be done based on telemetry and MEDLI2 data, some phenomena of EDL are best depicted through sight and sound. For example, the dynamics of parachute inflation are complex and nonlinear, and cannot be fully resolved using acceleration data recorded by the IMU. EDL Cameras were added to the Mars 2020 mission in order to improve engineers' understanding of events like these, as well as adding to the public's excitement about the climactic events of EDL.

This subsystem, containing six cameras and a microphone, is spread out across the EDL system in order to capture imagery of all the key events from diverse vantage points. These
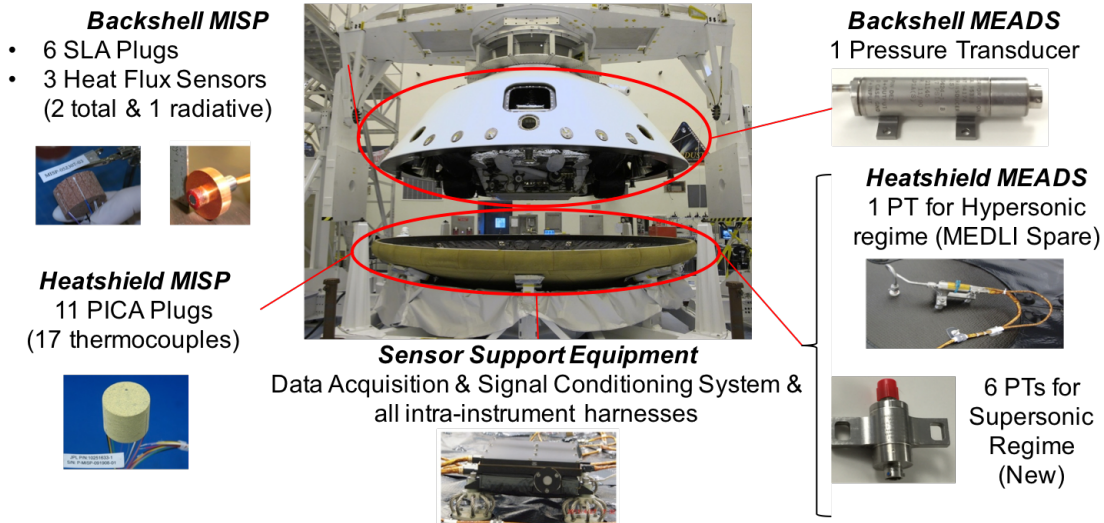
Figure 22. **The MEDLI2 sensor suite will characterize the aerodynamic and aerothermal environments and TPS performance in key regions of the Mars 2020 aeroshell. The addition of backshell instrumentation, including heat flux sensors and heat shield pressure transducers tuned for the supersonic flight regime, add crucial data to the record that was begun by the MEDLI experiment on the MSL.**
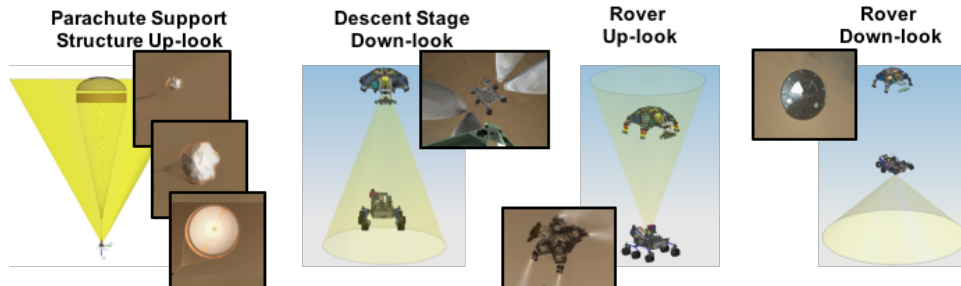

Figure 23. **EDL Cameras provide close-up imagery of key EDL events from a variety of vantage points.**

different cameras are depicted along with their notional fields of view in Figure 23.

The following hardware items constitute the EDL Camera suite:

- **Parachute Up-Look:** Three cameras are mounted to the parachute support structure at the aft end of the aeroshell. They face upward for imaging of the entire parachute deployment process including deployment, inflation, and operational dynamics from just before mortar fire until backshell separation.
- **Descent Stage Down-Look:** One camera, mounted on the underside of the Descent Stage, faces downward for imaging the rover dynamics during bridle descent and mobility deployment. This camera will also capture any Descent Stage main engine plume interactions with the Martian surface from skycrane through touchdown.
- **Rover Up-Look:** One camera, mounted on the top deck of the rover, faces upward to observe Descent Stage dynamics and plume characteristics from the beginning of the skycrane manuever through bridle-umbilical cut and the start of Descent Stage flyaway.
- **Rover Down-Look:** One camera, mounted on the side of the rover, faces downward to observe the release of the heatshield while hanging on the parachute. Following heatshield separation, this camera will observe the Martian surface from powered flight through the conclusion of the

skycrane maneuver and touchdown event.
- **Microphone:** One microphone, attached to the side of the rover, captures sounds from critical events such as the mortar fire of the parachute bag, the firing of Mars Lander Engines, the contact made with the Martian surface at touchdown, and the cutting of the bridles before Descent Stage flyaway.

The design philosophy taken in development of EDL Cameras is to minimize interactions between the EDL Camera subsystem and the Mars 2020 flight system during the execution of EDL. Aside from EDL Timeline flight software actions, which toggle power switches to supply or remove power to EDL Camera components, no other flight software commands are sent to this subsystem, nor will telemetry or imagery be collected during EDL. Only once the rover is safely on the Martian surface will flight software command the preparation and downlink of EDL Camera imagery.

6. NOTEWORTHY CHALLENGES

Heat Shield Static Test Failure

Heatshield (HS) #1 failed during the M2020 Aeroshell static test in April 2018. The MSL flight spare HS, which was designated as the flight unit for M2020, passed both the MSL static test and Spacecraft Thermal Vacuum test, as well as

survived handling operations. However, during the M2020 Aeroshell static test, the HS failed at 118% of the Flight Limit Load (the target load was 120% of the Flight Limit Load). A crack that ran circumferentially around the outer face sheet was only discovered after the test configuration was disassembled, as the airbag that applied the load to the HS hid the damage. The backshell, though part of the Aeroshell static test, was undamaged.

A Failure Review Board was convened to investigate the HS#1 incident and generate recommendations for the fabrication and manufacturing of HS#3. While no single cause was deemed responsible for the failure, several contributing factors were identified. First, workmanship quality issues plagued the composite, resulting in degraded material properties including poor bonding between the core splice and the face sheets, a high percentage of face sheet porosity, and the presence of interlaminar microcracking in the face sheets. Secondly, a design flaw created areas of concentrated stress, with a face sheet ply drop occurring at the location of peak stress. Third, non-uniform loading from the airbag used in the static test resulted in higher stresses on sections of the HS, leading to an overtest. Finally, the possibility of damage due to thermal cycling was considered.

With these contributing factors in mind, a few minor design changes were incorporated for HS#3. To begin, the HS#3 design was based on the successful HS#2 (the MSL Flight HS). This design included the use of flex core as opposed to the rigid hex core, as well as a renovated shoulder geometry design intended to accommodate the use of PICA as opposed to SLA-561V. The design updates inspired by the HS#1 failure include thicker face skins, redistributing the face sheet ply drop over a larger area, moving from circumferential tape to fabric plies near the edge, using a new core splice adhesive, and using a slitted honeycomb as opposed to a hand-perforated core. These design changes have an overall minimal impact on EDL performance, though the mass and material property changes are actively being incorporated into analyses. Furthermore, a few changes were made in the manufacturing processes, with the intent to address the material property degradation issues raised by the Failure Review Board. These changes improve breathing during the curing process and reduce the risk of inducing thermal damage to the HS.

Overall, this event will have a minimal impact to Assembly, Test, and Launch Operations (ATLO) activities. According to the original plan, JPL would receive HS#1 from Lockheed Martin in December 2018 for Vehicle Stack and Environments testing, and return the HS to the contractor in June 2019 for MEDLI2 and PICA integration and test (I&T). In the updated plan, JPL will receive a repaired HS#1 in the same timeframe for ATLO testing, and Lockheed Martin will manufacture HS#3 to meet a deadline of MEDLI2 and PICA I&T.

Mars Helicopter Accommodation

Mars 2020 will carry a helicopter experiment to the surface. Though it will not have functionality or testing to compliment this mission, the helicopter could pioneer future paired missions that involve short range scouting by a future version. This component will be treated here in how the impact on mission EDL was quantified and incorporated into the hazard assessment for a region.

The abundance of rocks in a local area is described by the concept of the rock Cumulative Fractional Area (CFA). It is
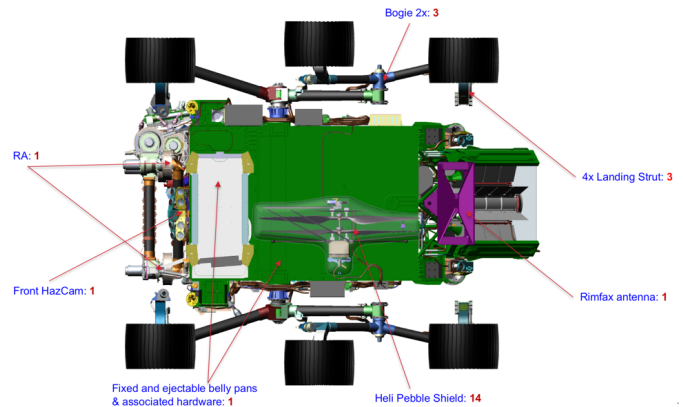

Figure 24. **Rover bellypan showing helicopter pebble shield**

a percentage that specifies the fraction of an area covered by rocks of any size; 10% CFA means that 10% of the area is covered by rocks of any size. An exponential curve based off of Viking and Mars analog sites on Earth show the relative abundance of different rock sizes. [21] A 10% CFA is expected to have a consistent fraction of rocks between 1-2 m in diameter, for instance. This relationship allows one to estimate the percentage of rocks, of a dangerous size, within the area specified by a CFA value.
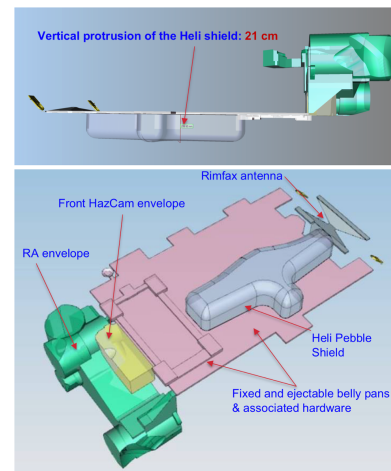

Figure 25. **Helicopter pebble shield leads to additional vertical protrusion**

Rocks become exponentially more abundant as their diameter decreases so the placement of the helicopter on the lower belly of the rover strongly increases the risk of impacting a rock. Currently roughly 0.5% of the estimated landed risk is associated with the addition of the helicopter experiment. The addition of TRN has allowed a reasonable system performance of approximately 99% by side-stepping hazards but it should be recognized that roughly half of this system risk is associated with a rock strike to the current allocated area for the helicopter.

Analyses used to quantify the risk of a rock strike assume that any contact to the rover, that is not a wheel, is a mission ending event. A crushed helicopter could prevent the rover from leaving the landed location or a struck landed strut could damage the operation of the wheels. Traversal is critical for the mission so any non-wheel contact is considered as
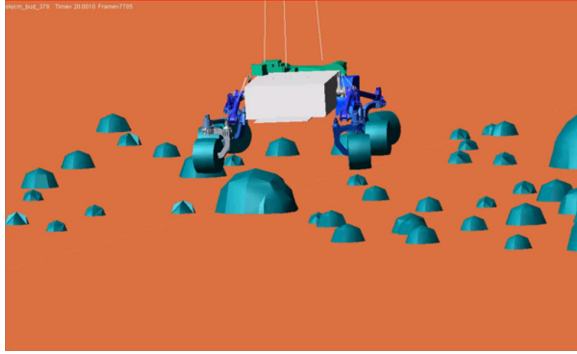
16

mission ending.

Figure 26. **ADAMS modeling of touchdown dynamics**

ADAMS high-fidelity models of the mobility system and outer mold line of the rover were used in landing Monte Carlos, as shown in Figure 26, to quantify areas contacted by a rock field generated to follow the expected exponential character of a specified CFA (i.e. 7%, 8%, and 10%). A Poisson approximation using the number of rocks, of a dangerous size, over the region vs the expectation of at least one rock, of a dangerous size, would appear over the footprint of the rover was also used. The approximation was similar to prior work done for InSight [22] and the MSL [23] but the mobility rock tolerance could be tuned by the high-fidelity ADAMS work to provide consistent risk estimates over a wide range of CFA values.

7. CONCLUSIONS AND FUTURE WORK

Making use of the heritage derived from the MSL's successful landing and surface operations, Mars 2020 incorporates new technologies and lessons learned to land a more massive and capable rover on terrain with greater scientific value. Though much of the EDL design and execution is inherited from the MSL, a number of updates and improvements have been made, noticeably the inclusion of a strengthened parachute and the Range Trigger, TRN, EDL Cameras, and MEDLI2.

Additionally, a number of risk mitigation strategies have been employed, addressing areas for improvement on the MSL. These include R&D efforts focused on characterizing the stresses on parachutes incurred during deployment, understanding negative ramifications and possible saturation on the IMU following parachute deployment, investigating the sandy radar phenomenon, and improving the terrain gravity map.

Despite the challenges delineated in this paper, the EDL development is on schedule for a launch in July 2020 and landing in February 2021. The complex system described above will not only allow for a larger landed rover that can travel farther across more scientifically-appealing terrain, but also provide a platform to carry out the search for signs of life, accomplish the potential first leg of sample return, and prepare for a human expedition to Mars.

REFERENCES

[1] J. Mustard and et al, "Report of the Mars 2020 Science Definition Team," *Mars Exploration Program Analysis Group (MEPAG)*, 2013.

[2] R. Prakash and et al, "Mars Science Laboratory Entry, Descent, and Landing System Overview," *IEEEAC Paper*, no. 2008-1531, 2008.

[3] A. Steltzner, "Mars Science Laboratory Entry, Descent, and Landing System Overview," *AAS Paper*, no. 13-236, 2013.

[4] J. A. Grant, M. P. Golombek, S. A. Wilson, K. A. Farley, K. H. Williford, and A. Chen, "The science process for selecting the landing site for the 2020 Mars rover," *Planetary and Space Science*, 2018.

[5] K. A. Farley and K. H. Williford, "Seeking signs of life, and more: NASA's Mars 2020 mission," *Eos*, no. 98, 2017.

[6] A. Huertas, Y. Cheng, and L. H. Matthies, "Real-time hazard detection for landers," 2007.

[7] C. W. Chen and B. D. Pollard, "Radar Terminal Descent Sensor Performance During Mars Science Laboratory Landing," *Journal of Spacecraft and Rockets*, vol. 51, no. 4, pp. 1208–1216, 2014.

[8] K. M. Górski, B. G. Bills, and A. S. Konopliv, "A high resolution mars surface gravity grid," *Planetary and Space Science*, vol. 160, pp. 84 – 106, 2018.

[9] I. G. Clark and C. L. Tanner, "A Historical Summary of the Design, Development, and Analysis of the Disk-Gap-Band Parachute," Tech. Rep. 2017, 2017.

[10] C. L. Tanner and I. G. Clark, "Overview of the Mars 2020 Parachute Risk Reduction Activity," Tech. Rep. 2018, 2018.

[11] C. O'Farrell, C. Karlgaard, J. Tynis, and I. Clark, "Overview and Reconstruction of the ASPIRE Project's SR01 Supersonic Parachute Test," Tech. Rep. 2018, 2018.

[12] C. O'Farrell, B. S. C. Karlgaard, J. Tynis, and I. Clark, "Overview of the ASPIRE Project's Supersonic Flight Tests of a Strengthened DGB Parachute," Tech. Rep. 2019, 2019.

[13] P. Brugarolas, "Mars 2020 Entry Descent and Landing Guidance Navigation and Control," *AAS GNC Conference*, 2017.

[14] A. Johnson, S. Aaron, J. Chang, Y. Cheng, J. Montgomery, S. Mohan, S. Schroeder, B. Tweddle, N. Trawny, and J. Zheng, "The Lander Vision System for Mars 2020 Entry, Descent, and Landing," *American Astronautical Society*, no. 17-036, 2018.

[15] G. F. Mendeck and G. L. Carman, "Guidance Design for Mars Smart Landers Using the Entry Terminal Point Controller," *AIAA Atmospheric Flight Mechanics Conference and Exhibit*, no. 2002-4502, 2002.

[16] D. W. Way, "On the use of a range trigger for the Mars Science Laboratory Entry, Descent, and Landing," *IEEEAC*, no. 1142, 2011.

[17] S. Dutta and D. W. Way, "Comparison of the Effects of Velocity and Range Triggers on Trajectory Dispersions for the Mars 2020 Mission," *AIAA Atmospheric Flight Mechanics Conference*, no. 2017-0245, 2017.

[18] H. Hwang, D. Bose, H. Wright, M. S. Todd R. White, J. Santos, C. D. Karlgaard, C. Kuhl, T. Oishi, and D. Trombetta, "Mars 2020 entry, descent, and landing instrumentation (medli2)," *46th AIAA Thermophysics Conference, AIAA AVIATION Forum*, no. 2016-3536.

[19] M. Schoenenberger, J. V. Norman, C. Karlgaard, P. Kutty, , and D. Way, "Assessment of the reconstructed aerodynamics of the mars science laboratory entry vehicle," *Journal of Spacecraft and Rockets*, vol. 51, no. 4, pp. 1076–1093, 2014.

[20] M. M. Deepak Bose, Todd White and K. Edquist, "Reconstruction of aerothermal environment and heat shield response of mars science laboratory."

[21] M. Golombek and D. Rapp, "Size-frequency distributions of rocks on Mars and Earth analog sites: Implications for future landed missions," *Journal of Geophysical Research*, 1997.

[22] M. Golombek, D. Kipp, N. Warner, and et al, "Selection of the InSight Landing Site," *Space Sci Rev*, vol. 211, no. 5, 2017.

[23] M. Golombek, J. Grant, D. Kipp, and et al, "Selection of the Mars Science Laboratory Landing Site," *Space Sci Rev*, vol. 170, pp. 641–737, 2012.

BIOGRAPHY

Adam P. Nelessen is a Systems Engineer at JPL, where he focuses on the design and architecture of EDL systems. Adam is an EDL Systems Engineer for the Mars 2020 mission, as well as the Principal Investigator for a Technology Development initiative examining the use of aerocapture to deliver Small Satellites to orbit. He received a JPL Voyager Award for his work in the formulation of future Mars Sample Return missions. He holds a B.S. degree in Mechanical Engineering from Northern Arizona University, and a M.S. degree in Aerospace Engineering from the Georgia Institute of Technology.

Chloe Sackier is a Systems Engineer at JPL working in the Entry, Descent, and Landing Systems and Advanced Technologies group. She has a B.S. in Aerospace Engineering from the Massachusetts Institute of Technology.

Ian G. Clark is a Systems Engineer at JPL, and a specialist in the area of Planetary Entry, Descent, and Landing (EDL). Dr. Clark is the recipient of a number of awards including the Presidential Early Career Award for Scientists and Engineers, the JPL Lew Allen Award, and the JPL Explorer Award. He was Principal Investigator of the Low-Density Supersonic Decelerators project and the ASPIRE Parachute Test Program. He holds B.S., M.S., and Ph.D. degrees in Aerospace Engineering from the Georgia Institute of Technology, where he also previously served as a Visiting Assistant Professor.

Paul Brugarolas Paul Brugarolas joined the Jet Propulsion Laboratory in 1997. Over the last 20 years, he has been involved in the design and development of GNC systems for a wide range of missions (including the Mars Science Laboratory, the Spitzer Space Telescope, the Shuttle Radar Topography Mission, and the Cassini Mission), and research and technology developments. Dr. Brugarolas is currently the chief engineer for the GNC subsystem for the Mars 2020 project.

Gregorio Villar is a Systems Engineer at JPL working in the Entry, Descent, and Landing Systems and Advanced Technologies group. Gregorio previously worked on the MSL EDL team and has been a member of the Mars 2020 EDL team since Pre-Phase A (2013). Gregorio has a B.S. in Physics from the California State Polytechnic University, Pomona and a M.S. in Astronautical Engineering from the University of Southern California. When he is not engineering, you can find Gregorio either conducting wizardry, competing in chess, creating music, or traveling the world.

Allen Chen is a systems engineer in the Entry, Descent, and Landing Systems and Advanced Technologies group. He is currently the Entry, Descent, and Landing Phase Lead for the Mars 2020 project. Prior to that, he spent a really long time working on the Mars Science Laboratory EDL team. He holds S.B. and S.M. degrees in Aeronautics and Astronautics from the Massachusetts Institute of Technology and an M.B.A. from the University of California, Los Angeles.

Aaron Stehura is a Systems Engineer at NASA's Jet Propulsion Laboratory. Mr. Stehura has held a variety of roles on the Mars Science Laboratory and Mars 2020 projects since 2010, primarily related to the Entry, Descent, and Landing phase of both missions. He holds bachelor's and master's degrees from Cornell University.

Richard Otero has been a member of the EDL Systems and Advanced Technologies Group, at the Jet Propulsion Laboratory, since 2011. He is currently in charge of landed hazard map creation for prospective M2020 sites and co-manages the M2020 Council of Terrains. Richard received a MS in Aerospace Engineering in 2009, a MS in Computer Science in 2010, and his PhD in Aerospace Engineering in 2012; all from Georgia Tech. He received his BS in Computer Science from SUNY New Paltz. He has been an Alfred P. Sloan Foundation Ph.D. Scholar, GEM fellow, and Time Person of the Year for 2006.

Erisa Stilley is currently working on the EDL systems team for Mars 2020. Previously, she enjoyed flying the Curiosity spacecraft to Mars, and planning drives for the rover once safely on the surface. Erisa grew up in northeastern Missouri. She has an MS in Aerospace Engineering from MIT and a BS in Mechanical Engineering from the University of Miami, Florida. She spent a summer volunteering with Engineering Ministries International in Colorado Springs before moving to Pasadena to work at JPL full-time.

David Way is an Aerospace Engineer in the Atmospheric Flight and Entry Systems Branch at the NASA Langley Research Center. His area of expertise is flight mechanics and modeling and simulation of planetary entry systems. Dr. Way has a Ph.D. and M.S. in Aerospace Engineering from the Georgia Institute of Technology and a

B.S. in Aerospace Engineering from the United States Naval Academy, Annapolis.

*   ***Karl Edquist*** *has worked at NASA Langley Research Center since 2000. He received his Bachelor's and Master's degrees in Aerospace Engineering from the University of Colorado and the University of Maryland, respectively. He specializes in aerodynamic and aerothermodynamic analysis of planetary entry vehicles for NASA science missions and technology development projects. Currently, he is Aerothermal Lead for NASA's Mars 2020 project and the lead for Propulsive Descent testing in the Langley Unitary Plan Wind Tunnel.*

*   ***Swati Mohan*** *got her B.S from Cornell University in Mechanical and Aerospace engineering in 2004. She got her PhD from MIT Aero/Astro in 2010. Swati's PhD was in the MIT Space Systems Laboratory on the SPHERES project. She joined JPL in 2010 and has worked various projects since joining such as Cassini, Grail, and OCO-3. Swati is currently the Lead GN&C Systems Engineer on the M2020 mission, specifically working on EDL and adding Terrain Relative Navigation. She is also the Co-Founder and Manager of JPL's Small Satellite Dynamics Testbed.*

*   ***Cj Giovingo*** *is a Systems Engineer at JPL. They are currently working on the Mars 2020 EDL Systems team, in charge of the verification and validation of EDL Communications and the EDL backup flight software, Second Chance. Cj came to JPL in 2014 following a career as a political organizer, skills which are surprisingly transferrable to systems engineering. They received a BS in Astronautical Engineering from Capitol Technology University in Maryland and are in the process of completing an MS in Astronautical Engineering from the University of Southern California.*

*   ***Mallory Lefland*** *is a Systems Engineer in the Flight System Systems Engineering group at NASA JPL. She is currently working on the Mars 2020 Entry, Descent, and Landing team, focusing on flight system design verification. She has previously worked on the Flight System Systems Engineering team for Mars 2020 and the Engineering Operations team for the Mars Science Laboratory Curiosity Rover. Mallory has a B.S. in Aerospace Engineering from the Georgia Institute of Technology. In her free time, you'll find her leading mini-yoga sessions and taking far too many polaroid pictures.*